JOURNAL OF PROPULSION AND POWER
Vol. 9, No. 6, Nov.–Dec. 1993

Erosive Burning in Solid Propellant Motors

J. C. Godon,* J. Duterque,* and G. Lengellé†
Office National d'Etudes et de Recherches Aérospatiales, BP72, F-92322 Châtillon, France

The erosive burning of ammonium perchlorate (AP) inert binder propellants is considered both experimentally and from the modeling viewpoint. The full modelization, developed earlier, is applied for various scales and reveals a pronounced scale effect. From these numerical results and preceeding others, a correlation law is thus extracted which gives an estimate of the wall shear stress with strong injection. This is the root of the concise model, in which a local one-dimensional description of the wall zone (including the combustion flame) is fed with the sole knowledge of the mean specific mass flow rate in the channel above the propellant. It shows that the propellant normal burning rate is the main parameter which influences the erosive burning response. Furthermore, this normal burning rate has a direct influence on the threshold for erosive burning. From this simple concise model, the influence of the scale upon the threshold is included in a universal correlation with appropriate nondimensional parameters, as found previously with complex turbulent flow computations.

Nomenclature

A = channel cross-sectional area
C = channel wetted perimeter
C_f = skin friction coefficient with injection
C_{f0} = skin friction coefficient without injection
c_{pg} = heat capacity
D = diameter
D_h = hydraulic diameter
f = damping coefficient
h = specific enthalpy
$\tilde{h}$ = stagnation enthalpy
J_h = diffusional flux of enthalpy
K = mixing length constant
k = proportionality constant in the flame height criterion
L = grain length
L_m = mixing length
$\dot{M}$ = total mass flow rate
$\dot{m}_p$ = pyrolysis specific mass flow rate
P = pressure
Pr = Prandtl number
Q_f = energy release in the flame
Q_p = heat of pyrolysis
r_p = propellant burning rate
Sc = Schmidt number
T = temperature
u = velocity in the longitudinal direction
v = velocity normal to the surface
x = streamwise coordinate
y = coordinate normal to the surface
δ = viscous layer thickness
μ = dynamic viscosity
ρ = specific mass
τ = shear stress

Subscripts
f = relating to the flame
fad = for the adiabatic flame temperature
lam = laminar component
lim = at the end of the summation
p = relating to the propellant surface
tur = turbulent component

Received May 9, 1991; presented as Paper 91-1865 at the AIAA 27th Joint Propulsion Conference, Sacramento, CA, June 24–26, 1991; revision received Feb. 2, 1993; accepted for publication April 2, 1993.

*Scientist, Energetics Department.
†Senior Scientist, Energetics Department. Member AIAA.

I. Introduction

THE curve giving the burning rate of a solid propellant, with respect to the pressure, is the main entry to compute the operating of a motor. For AP-based propellants, the burning rate level and the pressure exponent are set by the oxidizer particule size, total mass fraction, and additives to meet the needs of a project. But in some motors, it can be observed that the burning rate, connected with the choice of the propellant, escapes from its normal law. The so-called erosive burning is generally characterized by a sometimes very important enhancement of the burning rate in parts of the grain where the combustion surface is exposed to high specific mass flow rates. The work presented here was carried out for several years and aims at modeling the phenomenon to easily predict, by taking into account the specific propellant and grain geometry, its occurrence and impact.

II. Previous Erosive Burning Modeling

In recent years several works have dealt with the modeling of erosive burning. Renie and Osborn[1] associate an approximate turbulent boundary-layer approach and a detailed description of composite propellant flames. King[2,3] retains a fairly approximate empirically-based turbulent flow description with a detailed modeling of diffusion flames for composite propellants, as well as premixed flames for homogeneous propellants. Kuo[4,5] performs a detailed numerical calculation of a turbulent (with a kinetic energy-dissipation rate model) shear flow, coupled to a premixed flame. Beddini[6] stresses the shear flow turbulent modeling, coupled to a premixed single-step flame description.

The approach that was developed here is similar in spirit to the above-mentioned works, retaining the idea proposed earlier[7] of erosive burning being due to the penetration of the flow turbulence within the flame height. It keeps the same degree of sophistication in both the flow and the propellant flame modeling. A numerical turbulent flow description was performed with the Spalding-Patankar method, and the zone close to the surface (of the order of 100 μ), which contains the propellant diffusion flame, was described with the Couette approximations.[8] The first results were favorably confronted with experimental measurements.

III. Wall Zone Description

In most motors, the propellant surface delineates a channel in which the combustion products are flowing. The flame zone

(a few tens of microns above the solid surface) is very small compared to the channel size, and is generally contained in the laminar sublayer so that the propellant burns according to its normal burning rate law. When the velocity gradients become more important, the flow turbulence penetrates within the flame height and creates an enhancement of the transport coefficients and of the heat flux coming back to the surface, with a consequent increase in the propellant burning rate.

A simple one-dimensional description of the wall zone, which contains the propellant flame, suffices to evaluate the burning rate under erosive regime. The Couette equations

$$\mathring{m}_p = \rho_p r_p = \rho(y)v(y) \tag{1}$$

$$\mathring{m}_p u(y) = \tau(y) - \tau_p - y\frac{dP}{dx} \tag{2}$$

$$\mathring{m}_p \tilde{h}(y) = \mathring{m}_p h_p - [J_h(y) - J_{h0}] + u(y)\tau(y) \tag{3}$$

taking into account that u is of the order of v, and that the longitudinal gradients are negligible with respect to the transverse ones, are solved from the surface with the Runge-Kutta-Gill method. The velocity profile is obtained from the momentum conservation equation [Eq. (2)], knowing the wall shear stress τ_p. The energy conservation equation [Eq. (3)] determines the temperature profile between the surface and downstream of the flame by iterations on $\mathring{m}_p$. To evaluate the viscous shear stress

$$\tau = (\mu_{lam} + \mu_{tur})\frac{du}{dy} \tag{4}$$

the mixing length approach was adopted for the turbulent viscosity:

$$\mu_{tur} = \rho(y)L_m(y)^2\frac{du}{dy} \tag{5}$$

In the internal zone of the viscous layer, the mixing length is proportional to the height y above the surface

$$L_m(y) = Kf(y)y \tag{6}$$

with $K = 0.4$ and a damping coefficient

$$f(y) = 1 - \exp[-(y/a)(\tau/\tau_p)^n] \tag{7}$$

where

$$a = (26\mu_p/\sqrt{\rho_p\tau_p}) \tag{8}$$

and the value of n is adjusted to 0.7 in order to match experimental results for very strong injection rates (Fig. 7 of Ref. 8). In the external zone, the mixing length is bounded by a value proportional to δ (i.e., often the half-height of the channel):

$$L_m = 0.09\delta \tag{9}$$

The temperature profile is obtained from Eq. (3) with the specific enthalpy

$$h(y) = \tilde{h}(y) - u(y)^2/2 = h_p + c_{pg}[T(y) - T_p] \tag{10}$$

and the diffusional flux of enthalpy

$$J_h(y) = \left[\frac{\mu_{lam}(y)}{Pr_{lam}} + \frac{\mu_{tur}(y)}{Pr_{tur}}\right]\frac{dh}{dy} \tag{11}$$

which uses laminar and turbulent values of the Prandtl number. The term J_{h0} in Eq. (3) is the wall heat flux

$$J_{h0} = J_{hp} = -\mathring{m}_p Q_p \tag{12}$$

between the surface and flame, and becomes

$$J_{h0} = J_{hp} - \mathring{m}_p Q_f \tag{13}$$

beyond the flame. The flame height criterion allows one to locate the point where the energy Q_f is liberated by the combustion. For a gaseous species diffusion process, it is obtained[8]

$$\mathring{m}_p D_0^2 = 2k\int_0^{y_f}\left[\frac{\mu_{lam}(y)}{Sc_{lam}} + \frac{\mu_{tur}(y)}{Sc_{tur}}\right]dy \tag{14}$$

with D_0 associated to the AP particle size, and k a proportionality coefficient related to the propellant. With the knowledge of the propellant normal burning rate and its adiabatic flame temperature T_{fad}, the summations of Eqs. (3) and (14), under normal burning conditions ($u = 0$) and with laminar transfer parameters, yields the value of k.

In the presence of a flow, the parallel summation of the velocity and temperature profiles [Eqs. (2) and (3) coupled with Eq. (14)], is carried out, taking into account the turbulent transfer parameters, and is stopped at a height y_{lim} above the surface (about 100 μ), large enough to contain the flame zone, but sufficiently small to remain within the Couette hypothesis. A proper value of τ_p gives a good description of the viscous turbulent flow developed above the strongly injecting propellant surface, and the erosive mass flow rate $\mathring{m}_p$ allows matching of the combustion products enthalpy. In order to have a self-contained model, only the knowledge of the wall shear stress value with strong blowing is required, but here is the main difficulty of the modelization.

IV. Full Modelization and the Concise Model

The first step[8] was to couple the one-dimensional wall zone description with a full turbulent two-dimensional description of the whole flow in which the Navier-Stokes equations, simplified with the shear flow approximations, were solved with the Patankar and Spalding method. In the wall zone, the iteration on the values of τ_p and J_{hp}, directly related to $\mathring{m}_p$ in Eq. (12), is carried until the velocity and temperature profiles match those of the full description (Fig. 1). The erosive burning rate is then immediately obtained from Eq. (12).

As an example of the performed applications, the full modelization was used to study the motor scale effect on erosive burning and at the same time to produce shear stress values for a large domain of flow Reynolds numbers. The computation takes into account three motor scales: 1) S1/1, 2) S1/10, and 3) S1/100 in a simple geometry, i.e., an axisymmetric grain with L and a port D (Fig. 2). In a first approx-

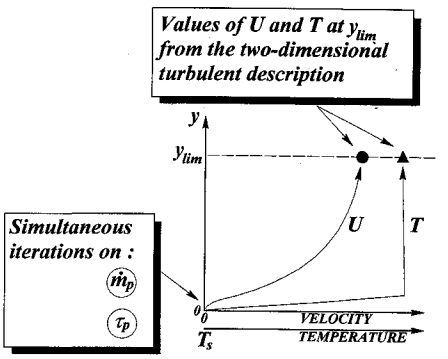

Fig. 1 Full modelization: coupling of the wall zone description with a two-dimensional viscous flow description.

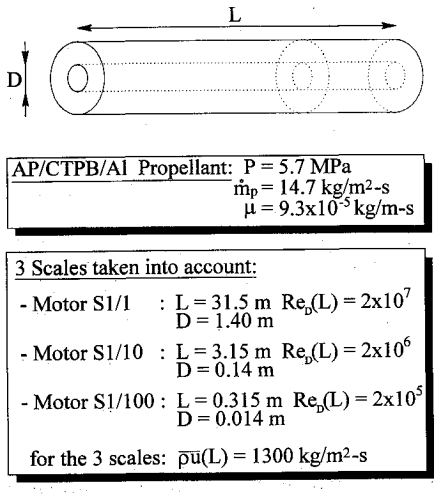

Fig. 2 Data for scale effect computations in axisymmetrical motors.

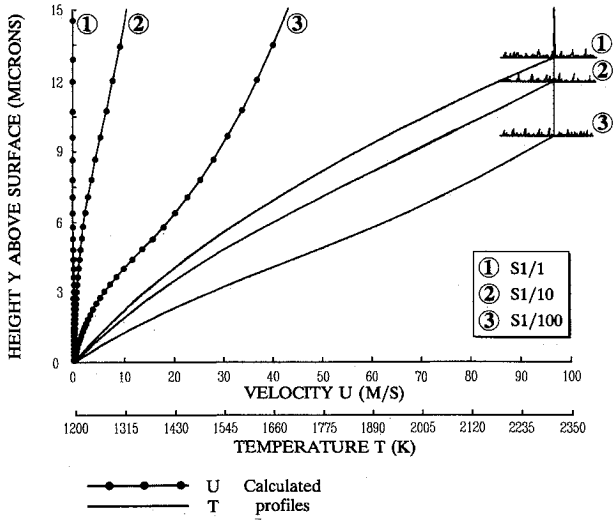

Fig. 3 Scale effect on the flame zone.

imation, the pressure gradient can be neglected and, for a given normal burning rate, $\dot{m}_p$ remains constant on the whole combustion surface. At the end of the grain, the mean specific mass flow rate

$$\overline{\rho u} = [\pi D L \dot{m}_p/(\pi D^2/4)] = (4L\dot{m}_p/D) \tag{15}$$

is independent of the motor scale, whereas the flow Reynolds number at L

$$Re_D(L) = (\overline{\rho u} D/\mu) = (4L\dot{m}_p/\mu) \tag{16}$$

is proportional to the grain size. The three detailed profiles (Fig. 3) predict that, for the S1/1 scale (solid booster), the velocity profile is blown away from the flame zone by the injection and there is no modification of the temperature profile. Then the propellant normal burning rate is preserved. On the contrary, for the S1/100 scale (slab motor), the velocity profile strongly penetrates the flame zone. The high turbulence level between surface and flame creates erosive burning conditions. It is then seen here that the same propellant has a different erosive behavior according to the motor scale (Fig. 4). The pressure, and therefore, the normal burning rate, are quite the same along the three grain geometries (P = 5.9–5.4 MPa). The computed results show that the propellant keeps a normal burning rate up to the end of the large grain where the mean specific mass flow rate is about 1300

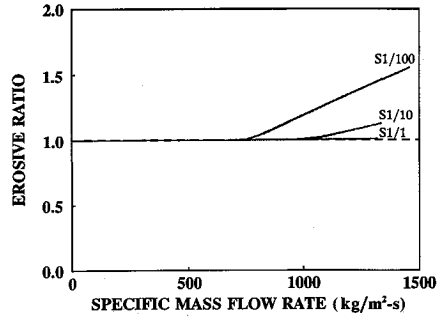

Fig. 4 Computed scale effect on the erosive behavior in axisymmetrical motors.

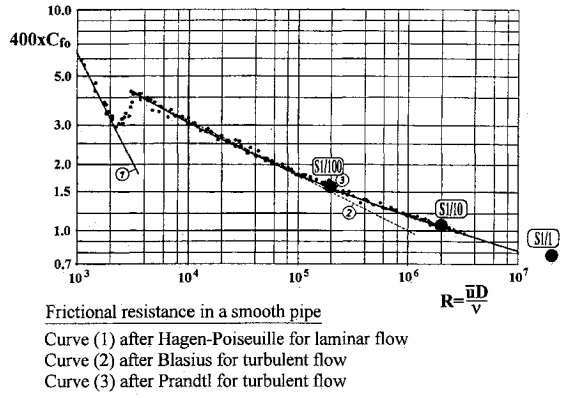

Fig. 5 Experimental skin friction coefficients in a pipe without injection and empirical laws.

kg/m²-s. In the small geometry, the erosive threshold is close to 700 kg/m²-s; at the motor exit, the burning rate increase is about 50% for a slightly higher mass flow rate (1450 kg/m²-s).

Experimental results for frictional resistance in smooth pipes are numerous and give empirical formulas valid in a large Reynolds number domain.[9] The values for C_{f0}, obtained for a flow computed without blowing in our three scales, are in accordance with these data for the two smaller geometries (Fig. 5) and for the large scale in the continuation of the Prandtl's universal law

$$(1/\sqrt{C_{f0}}) = 4 \log_{10}(Re_D 2\sqrt{C_{f0}}) - 0.8 \tag{17}$$

which will be used in the concise model with a flow Reynolds number Re_D at the considered axial location, and referred to the hydraulic diameter

$$D_h = 4(A/C) \tag{18}$$

The full modelization was used in many configurations to describe the viscous turbulent flow developed above an injecting propellant surface and to determine the wall shear stress

$$\tau_p = \tfrac{1}{2} C_f \overline{\rho u} \cdot \bar{u} \tag{19}$$

in various geometries, in a large range of flow Reynolds numbers, injection rates, and pressure gradients. The computed values of C_f are presented in Fig. 6 as a function of C_{f0} and of the injection ratio, defined as

$$B = (\dot{m}_p/\tfrac{1}{2} C_f \overline{\rho u}) \tag{20}$$

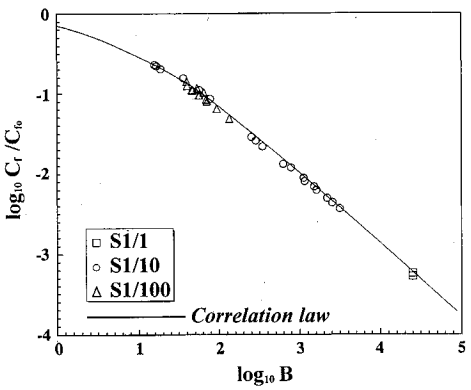

Fig. 6 Correlation of the full modelization for the wall shear stress results in a pipe with injection.

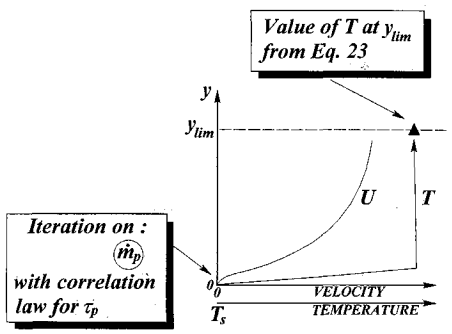

Fig. 7 Concise model: coupling of the wall zone description with a one-dimensional nonviscous flow description.

in accordance with the usual form.[7] To correlate these numerical results, the curve

$$(C_f/C_{f0}) = \{1 + \alpha[1 - \exp(-0.05B)]\}$$
$$[\mathscr{A}(1 + B)/B] \tag{21}$$

is adjusted with $\alpha = 0.5$. Thus obtained from the full modelization (which is too cumbersome for use in predicting a motor performance), this correlation law is the root of the concise model, which avoids the turbulent description of the whole flow.

Only the mean characteristic values of the main flow (as obtained from a one-dimensional computation) are now needed to evaluate the erosive burning. The pressure gradient in Eq. (2) is then

$$\frac{dP}{dx} = \frac{\mathring{M}\bar{u}}{A} \frac{\left[\frac{1}{A}\frac{dA}{dx} - \left(2 + \frac{\bar{u}^2}{c_p\bar{T}}\right)\frac{1}{\mathring{M}}\frac{d\mathring{M}}{dx}\right]}{\left(1 + \frac{\bar{u}^2}{c_p\bar{T}} - \frac{\mathring{M}\bar{u}}{AP}\right)} \tag{22}$$

with $\mathring{M}$ denoting the total mass flow rate in the channel. The initial value of $\mathring{m}_p$ determines the wall values J_{hp} [Eq. (12)] and τ_p [Eqs. (16–21)]. The simultaneous summation of the u and T profiles [Eqs. (2) and (3)] is carried out from the surface to a distance y_{lim} containing the propellant flame. The iteration on the $\mathring{m}_p$ value is repeated as many times as necessary to verify for $y = y_{\text{lim}}$:

$$c_pT(y_{\text{lim}}) = c_pT_{\text{fad}} - u(y_{\text{lim}})^2/2 \tag{23}$$

This simplified process (Fig. 7) constitutes the fastest tool to locally evaluate the propellant burning rate from a nonviscous flow description inside a complex grain geometry. It should be noted that this approach is similar to that of King[3,10] (Ref. 10 being a complete review of this author's work). However, the skin friction coefficient correlation [Eq. (21)] is believed to be of better quality, after being obtained from full numerical computations which match the experimental results for strong injection rates.[8]

V. Experimental and Concise Model Results for Erosive Burning Phenomenon

A part of the propellant erosive behavior (the relative enhancement of its burning rate with the specific mass flow rate) is experimentally obtained in the separated generator/sample device.[8] The more numerous tests are related to 80% AP—20% carboxyterminated polybutadiene (CTPB) propellants. Changes in pressure level, AP particle size, or additives use allow modulation of the burning rate from 9.9 to 30 mm/s. These experimental results (Fig. 8) clearly show the gradual influence of the normal burning rate on the erosive behavior; the faster the propellant, the lower the slope and level of erosion, and the higher the threshold.

The application of the concise model to an 80% AP—20% CTPB propellant uses the parameter values of Table 1. The pressure, which by itself has no true impact, is set at 7 MPa; the channel size, which has only small variations during the test, is set at 5 mm to eliminate the time dependence. The normal burning rate is the only parameter that was varied in the computations to obtain the erosive behaviors (Figs. 9 and 10) which are in overall proper agreement with the above-mentioned experimental results.

The same curves are presented in Fig. 11 for a larger range of theoretical normal burning rate values (2–30 mm/s). This plot combines the effect of the two most important parameters

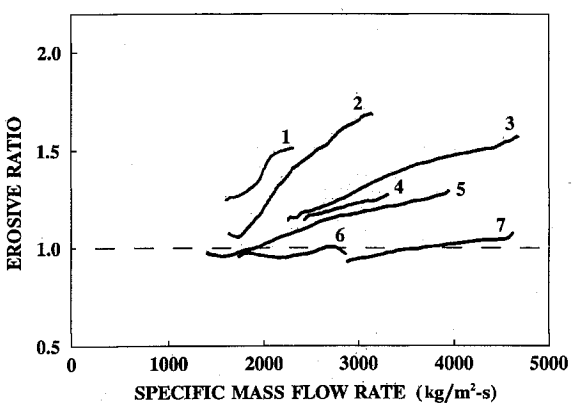

Fig. 8 Set of experimental results on the separated generator-sample device for AP/CTPB(/Al) propellants.

Table 1 Parameter's values for an 80% AP—20% CTPB propellant

ρ_p	=	1590 kg/m³
T_{fad}	=	2313 K
T_p	=	1200 K (average temperature between binder surface and AP premixed flame)
Q_f	=	-2.8×10^6 J/kg
Q_p	=	0.69×10^6 J/kg
c_{pg}	=	1900 J/kg-K
W_{mol}	=	28.8 to 21.9 kg/kmole (from combustion surface to flame and main flow)
μ_{lam}	=	$3.13 \times 10^{-7}T^{0.7}$ kg/m-s
Pr_{lam}	=	0.74–0.50 (from combustion surface to flame and main flow)
Sc_{lam}	=	0.98
Pr_{tur}	=	0.9
Sc_{tur}	=	0.8

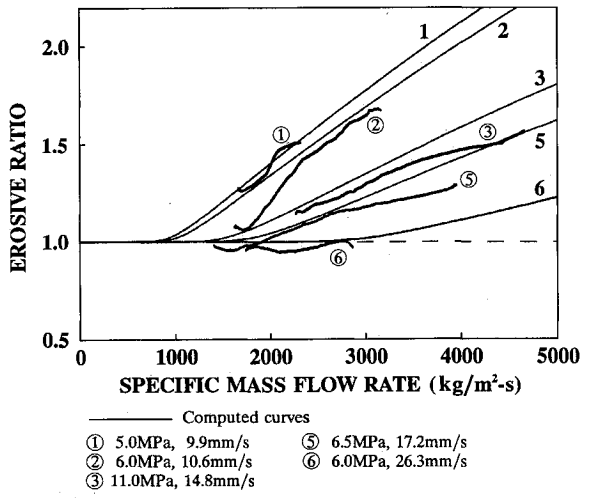

Fig. 9 Computed erosive behaviors and experimental results for AP/CTPB propellants.

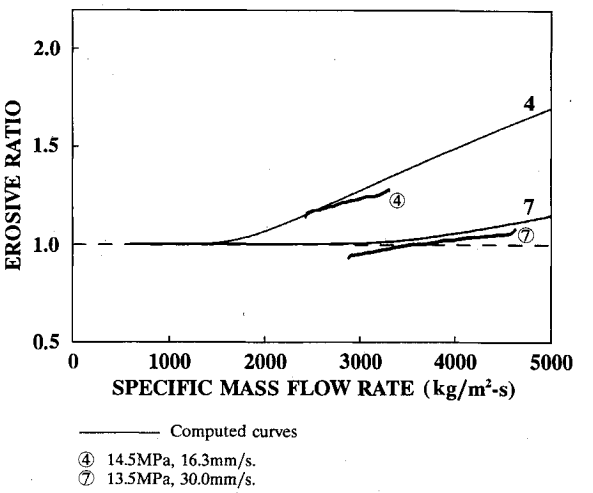

Fig. 10 Computed erosive behaviors and experimental results for AP/CTPB/Al propellants.

(specific mass crossflow rate and normal burning rate), and displays the main characteristics of the erosive phenomenon. The higher the burning rate, the closer to the surface is the flame and the lower the sensitivity is to the flow turbulence. The higher the specific mass flow rate, the more intense is the turbulence and the more pronounced is the erosive effect. King[10] has found the same tendencies both experimentally and from computation.

The erosive threshold concept which governs the phenomenon occurrence is a major concern to motor designers. In the model, a zone comprised between the 1–5% erosion level is defined to represent an erosive burning threshold experimentally detectable (Fig. 12). For low channel widths, numerous experimental setups or laboratory motors have been investigated under erosive conditions, particularly in this work (slab motors, axisymmetrical nozzleless motor, generator/sample setup). Although they are obtained under various geometry configurations (but with close channel sizes) and for different *AP* composite propellants (and even specific mixtures for extinguishable motor studies), the results display a clear correlation between erosive mass flow rate threshold and propellant normal burning rate (Fig. 13). The erosive threshold zone determined from the concise model is in good agreement with the above experimental observations.

The model is then applied to axisymmetric motors with theoretical radii of 5, 50, and 500 mm. The erosive domain determined by the normal burning rate, as on Fig. 13, is

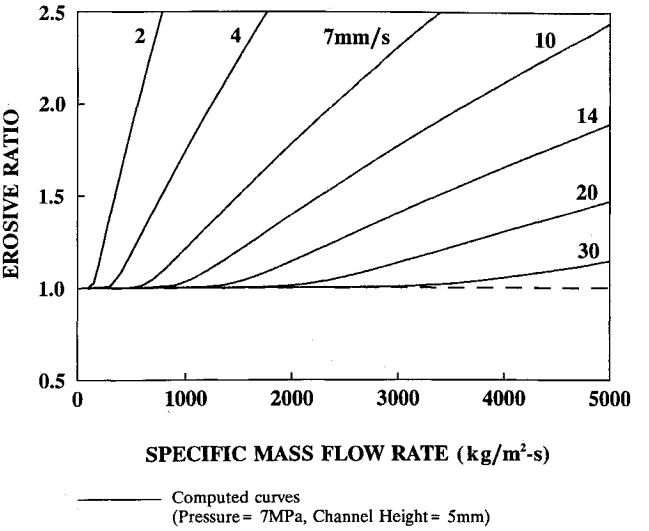

Fig. 11 Computed erosive behavior as a function of normal burning rate for AP/CTPB propellants.

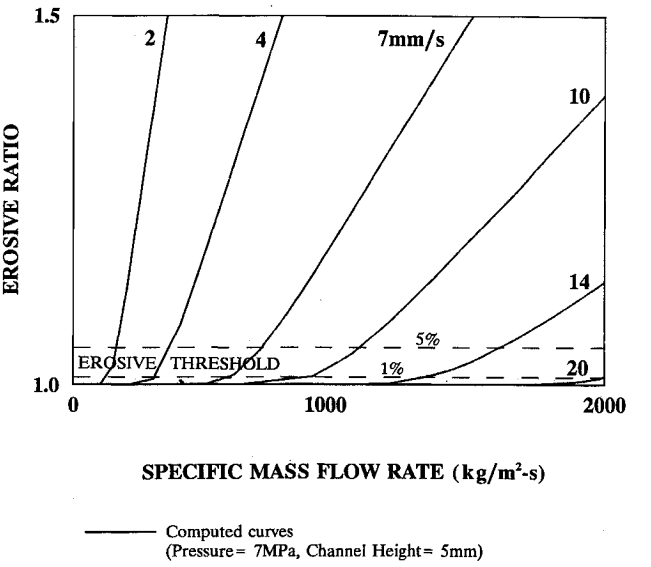

Fig. 12 Erosive mass flow rate threshold for AP/CTPB propellants as defined in the model.

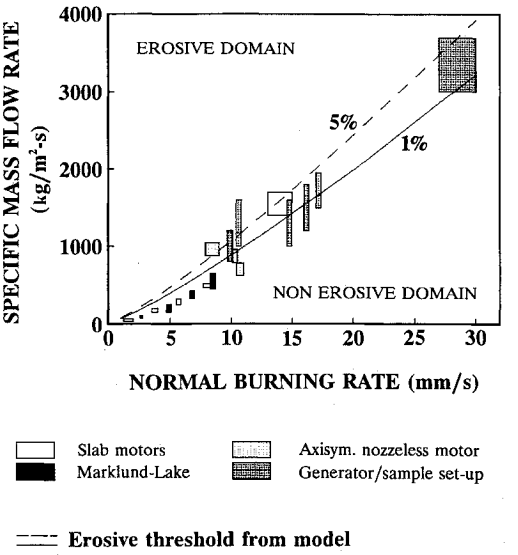

Fig. 13 Erosive mass flow rate threshold as from the concise model and various small scale experiments.

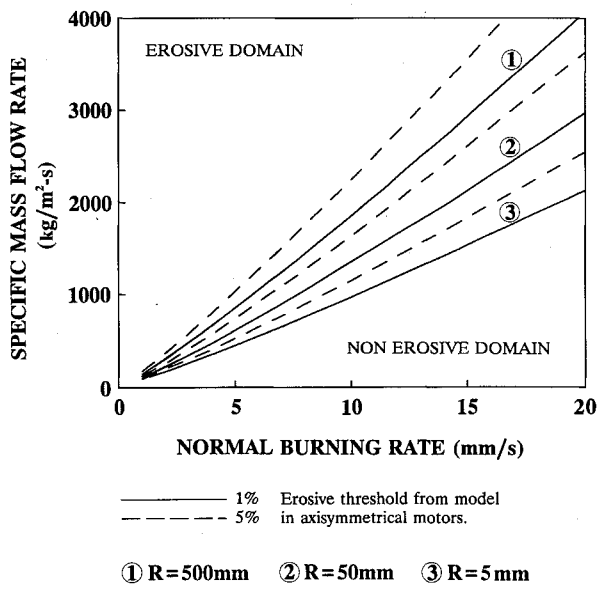

Fig. 14 Scale effect on the erosive mass flow rate threshold for AP/CTPB propellants.

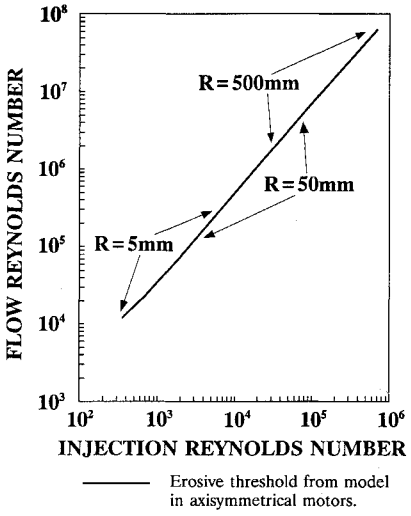

Fig. 15 Erosive threshold (2% erosion level) from the concise model, including scale effect for AP/CTPB propellants.

strongly modified by the channel size, thus revealing an important scale effect (Fig. 14). However, with a proper choice of nondimensional parameters,[6] i.e., flow Reynolds number and injection Reynolds number defined in the model as [it should be noted that in the present work these numbers are defined with mean $\overline{\rho u}$, as opposed to ρu centerline in Ref. 6, and with $\mu(T_p)$ at $T_p = 1200$ K]

$$Re_f = \frac{\overline{\rho u} D_h}{\mu(\bar{T})}$$

$$Re_i = \frac{\dot{m}_p D_h}{\mu(T_p)}$$

this scale effect collapses into a single curve (Fig. 15).

It should be observed that the concise model contains the idea that the viscous layers have evolved into fully developed flow in that part of the motor where erosive burning might occur. In particular, the reference (without injection) skin friction coefficient is that obtained for turbulent pipe flow (Fig. 5). The fact that the correlation based on diameter (and not on streamwise coordinate) reduces the results to a single curve on Fig. 15, as well as in the case of Beddini's results,[6] strengthens this viewpoint.

VI. Conclusion

The concise model, based on a correlation of the wall shear stress with strong blowing effects, uses average values for the flow and gives a possibility for a rapid local estimate of erosive burning levels within the scope of a nonviscous computation for a complex geometry grain.

In agreement with experimental observations, the model shows that the propellant erosive behavior depends mainly upon its normal burning rate. A direct influence of this normal burning rate upon the mass flow rate threshold for erosive burning is found. Furthermore, a strong influence of the motor scale is predicted, which however, can be incorporated into proper nondimensional parameters.

Acknowledgments

Work carried out under contract from the Direction des Recherches, Etudes et Techniques (DRET) and in relation with the Société Nationale des Poudres et Explosifs (SNPE). The experimental work was carried out with the help of F. Cauty and J. Hommel.

References

[1]Renie, J. P., and Osborn, J. R., "Erosive Burning," *AIAA Journal*, Vol. 21, No. 12, 1983, pp. 1681–1689.

[2]King, M. K., "A Model of the Effects of Pressure and Crossflow Velocity on Composite Propellant Burning Rate," AIAA/SAE/ASME 15th Joint Propulsion Conf., AIAA Paper 79-1171, Las Vegas, NV, June 1979.

[3]King, M. K., "Model for Prediction of Double-Base Propellant Burn Rate Including Cross-Flow Effects," *AIAA Journal*, Vol. 20, No. 10, 1982, pp. 1432–1439.

[4]Razdan, M. K., and Kuo, K. K., "Turbulent Flow Analysis and Measurements of Erosive Burning Rates of Composite Solid Propellants," *AIAA Journal*, Vol. 20, No. 1, 1982, pp. 122–128.

[5]Arora, R., Wu, X., White, F. X., and Kuo, K. K., "Erosive Burning of Composite Solid Propellants: Mechanism, Correlation and Grain Design Applications," *Journal of Spacecraft and Rockets*, Vol. 20, No. 1, 1983, pp. 43–48.

[6]Beddini, R. A., "Aerothermochemical Analysis of Erosive Burning in a Laboratory Solid-Rocket Motor," *AIAA Journal*, Vol. 18, No. 11, 1980, pp. 1346–1353; see also "Analysis of Injection-Induced Flows in Porous-Walled Ducts with Application to the Aerothermochemistry of Solid-Propellant Motors," Ph.D. Dissertation, Rutgers Univ., New Brunswick, NJ, 1981.

[7]Lengellé, G., "Model Describing the Erosive Combustion and Velocity Response of Composite Propellants," *AIAA Journal*, Vol. 13, No. 3, 1975, pp. 315–322.

[8]Godon, J. C., Duterque, J., and Lengellé, G., "Solid-Propellant Erosive Burning," *Journal of Propulsion and Power*, Vol. 8, No. 4, 1992, pp. 741–747.

[9]Schlichting, H., "Boundary Layer Theory," McGraw-Hill, New York, 1962.

[10]King, M. K., "Erosive Burning of Solid Propellants," *Combustion of Solid Propellants*, AGARD Lecture Series 180, Neuilly-sur-Seine, France, 1991, pp. 5-1–5-26.